Materials Today Bio 26 (2024) 101099

Contents lists available at ScienceDirect

Materials Today Bio

journal homepage: www.journals.elsevier.com/materials-today-bio

Enhancing tendon-bone integration and healing with advanced multi-layer nanofiber-reinforced 3D scaffolds for acellular tendon complexes

Chenghao Yu [a,b,c,d], Renjie Chen [e], Jinli Chen [b], Tianrui Wang [b], Yawen Wang [b,c,d], Xiaopei Zhang [b,c,d], Yuanfei Wang [f], Tong Wu [b,c,d,*], Tengbo Yu [a,**]

[a] Department of Orthopedic Surgery, Qingdao Municipal Hospital, University of Health and Rehabilitation Sciences, Qingdao, Shandong, 266071, China
[b] The Affiliated Hospital of Qingdao University, Qingdao Medical College, Qingdao University, Qingdao, Shandong, 266000, China
[c] Shandong Key Laboratory of Medical and Health Textile Materials, College of Textile & Clothing, Qingdao University, Qingdao, Shandong, 266071, China
[d] Institute of Neuroregeneration & Neurorehabilitation, Department of Pathophysiology, School of Basic Medicine, Qingdao University, Qingdao, Shandong, 266071, China
[e] Beijing Jishuitan Hospital National Center for Orthopaedics, Beijing, 102208, China
[f] Qingdao Stomatological Hospital Affiliated to Qingdao University, Qingdao, 266001, China

ARTICLE INFO

Keywords:
Nanofiber reinforcement
Acellular tendon complexes
Bioactive glass
Anterior cruciate ligament
Tendon-bone healing

ABSTRACT

Advancements in tissue engineering are crucial for successfully healing tendon-bone connections, especially in situations like anterior cruciate ligament (ACL) restoration. This study presents a new and innovative three-dimensional scaffold, reinforced with nanofibers, that is specifically intended for acellular tendon complexes. The scaffold consists of a distinct layered arrangement comprising an acellular tendon core, a middle layer of polyurethane/type I collagen (PU/Col I) yarn, and an outside layer of poly (L-lactic acid)/bioactive glass (PLLA/BG) nanofiber membrane. Every layer is designed to fulfill specific yet harmonious purposes. The acellular tendon core is a solid structural base and a favorable environment for tendon cell functions, resulting in considerable tensile strength. The central PU/Col I yarn layer is vital in promoting the tendinogenic differentiation of stem cells derived from tendons and increasing the expression of critical tendinogenic factors. The external PLLA/BG nanofiber membrane fosters the process of bone marrow mesenchymal stem cells differentiating into bone cells and enhances the expression of markers associated with bone formation. Our scaffold's biocompatibility and multi-functional design were confirmed through extensive *in vivo* evaluations, such as histological staining and biomechanical analyses. These assessments combined showed notable enhancements in ACL repair and healing. This study emphasizes the promise of multi-layered nanofiber scaffolds in orthopedic tissue engineering and also introduces new possibilities for the creation of improved materials for regenerating the tendon-bone interface.

1. Introduction

The anterior cruciate ligament (ACL), which plays a crucial role in the movement and stability of the knee joint, is prone to injuries [1]. The annual occurrence rate of these injuries varies from 30 to 78 per 100,000 individuals [2]. ACL injuries not only cause knee instability but also make the joint more susceptible to subsequent injuries and long-term degenerative effects [3]. Due to the limited ability of the ACL to regenerate after injury, it is commonly necessary to perform ACL restoration using either autograft or allograft techniques [4]. Although these procedures are widely employed, they have specific limitations, such as complications at the donor site in autografts and higher costs and failure rates in allografts [5–8]. Moreover, biomechanically substandard scar tissue development at the junction between the graft and the bone frequently hinders the recovery process [9,10].

The complex arrangement of collagen, minerals, and proteoglycans in the ligament-to-bone interface, which is organized in a hierarchical and gradient structure, presents considerable difficulty in ACL reconstruction [11–13]. Contemporary approaches in ligament tissue engineering strive to imitate this intricate arrangement yet frequently fail to

* Corresponding author. The Affiliated Hospital of Qingdao University, Qingdao Medical College, Qingdao University, Qingdao, Shandong, 266000, China.
** Corresponding author. Department of Orthopedic Surgery, Qingdao Municipal Hospital, University of Health and Rehabilitation Sciences, Qingdao, Shandong, 266071, China.
E-mail addresses: twu@qdu.edu.cn (T. Wu), ytb8912@hotmail.com (T. Yu).

https://doi.org/10.1016/j.mtbio.2024.101099
Received 17 February 2024; Received in revised form 20 May 2024; Accepted 21 May 2024
Available online 22 May 2024

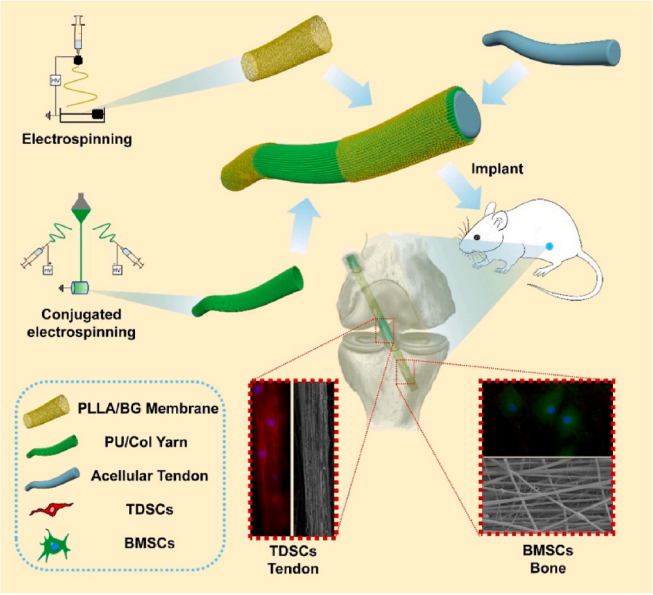

Scheme 1. Schematic illustration of the fabrication process and potential application of multi-layer nanofiber-reinforced three-dimensional scaffold for acellular tendon complex.

completely reinstate the operational and structural soundness of the original ACL insertion site [3,14,15]. The progress in tissue engineering has led to a change in emphasis towards developing scaffolds that imitate the natural extracellular matrix (ECM) environment and cater to the specific structural and compositional requirements of the tendon-bone interface [16–19]. Tang et al. produced a gradient book-shaped three-phase scaffold consisting of acellular tendon, fibrocartilage, and bone tissue [17]. Decellularization techniques can effectively remove cells from the original tissue used for scaffold preparation, which can greatly remove antigenic components and reduce the immunogenicity of scaffolds. In addition, the prepared scaffolds retained a large amount of ECM components and tissue strength to regulate the migration and differentiation of endogenous stem cells and achieve *insitu* tissue regeneration [20]. Yang et al. constructed a hydrogel based on gradient bimetal ions by adding copper and zinc ions [21]. In addition, Du et al. combined manganese silicate nanoparticles with tendon/bone-associated cells to fabricate an immunomodulatory multicellular scaffold for integrated tendon-bone regeneration [22]. The ECM microenvironment of the cellular niche is crucial because it can control the behavior and fate of stem cells. Among the approaches for producing scaffolds, electrospinning has the most advantages [23]. The scaffolds produced by this technology have the advantages of similar to natural ECM, cost-effectiveness, and wide practicality [24]. There has been a gradual shift from two-dimensional oriented nanofiber mats to three-dimensional oriented nanofiber bundles in the fabrication of tendon-mimicking scaffolds [25]. The scaffolds are also modified with growth factors or proteins such as type I collagen (Col I) to improve the effect of the scaffolds on the differentiation to tendon cells of stem cells [26,27]. In addition, the structure of random nanofibers could mimic the structure of bone and have a positive effect on bone regeneration. Bioactive substances such as bioactive glass (BG) have demonstrated potential due to their osteoconductive characteristics and capacity to promote osseointegration and bone regeneration [28,29]. Therefore, the combination of orientational yarn bundles that mimic tendon and random fiber membranes that mimic bone structure with constituents is advantageous for tendon-bone junction healing.

This study presents a novel method to address these difficulties by introducing a cutting-edge technique, including a multi-layered, nanofiber-reinforced, three-dimensional scaffold for acellular tendon complexes. The scaffold is intentionally constructed with a core made of acellular tendon, enveloped by a layer of polyurethane (PU) yarn containing Col I, and an exterior layer of poly (L-lactic acid) (PLLA) nanofibers combined with BG. This design not only mimics the structural and compositional differences found in the natural tendon-bone interface but also utilizes the unique characteristics of its constituent components. The acellular tendon core exhibits remarkable tensile strength, the PU/Col I yarn promotes the differentiation of mesenchymal stem cells (MSCs) into tendon cells, and the PLLA/BG nanofiber membrane stimulates the differentiation of MSCs into bone cells. This scaffold offers a new and perhaps more efficient alternative for improving tendon-bone healing in ACL restoration by imitating the natural tendon-bone contact in structure and function (Scheme 1).

2. Experimental section

2.1. Fabrication and characterization of acellular tendons

Rat leg tendons were harvested and subjected to a decellularization process involving 10 cycles of liquid nitrogen immersion and subsequent thawing in a 37 °C water bath for 10 min each. This method aimed to induce cellular lysis, thus producing acellular tendons. The tendons were then rinsed in phosphate-buffered saline (PBS) three times and treated with 0.1 % sodium dodecyl sulfate (SDS) and 1 % Triton X-100 to ensure complete removal of cellular components. Briefly, the tendons were immersed in a 0.1 % SDS solution, subjected to agitation for 3 h, and subsequently washed 3 times with deionized water. Tendons were immersed in a 1 % Triton X-100 solution for 1 h to eliminate any residual SDS, followed by thorough rinsing with shaking in PBS solution at 4 °C for 24 h to achieve the desired acellular tendon samples. The efficacy of decellularization was assessed through hematoxylin and eosin (H&E) (Solarbio) staining, DNA quantification, and gel electrophoresis. The fresh and decellularized tendons were embedded in paraffin and subsequently prepared for sectioning, followed by H&E staining of the paraffin sections. The H&E stained sections were observed by light microscopy. DNeasy Blood and Tissue Kit (QIAGEN) was used to purify tendon DNA according to the manufacturer's instructions. The DNA content was quantified using an ultramicro UV spectrophotometer. Purified DNA was subjected to electrophoresis on a DNA agarose gel to visualize the DNA content. These steps were crucial in confirming the preparation of a suitable acellular scaffold for subsequent scaffold fabrication.

2.2. Development of PU-Col I yarn and its cellular interaction

The PU/Col I yarns, critical for tendon mimicking, were fabricated using an advanced electrospinning technique. This involved dissolving PU and Col I in hexafluoroisopropanol and spinning the solution under specific electrospinning parameters. Briefly, PU was dissolved in hexafluoroisopropanol at a concentration of 6 wt%, and then Col I (1 wt%) was directly mixed into the solution for electrospinning. The solution was drawn into two 5-mL syringes and subsequently mounted onto the electrospinning apparatus for fiber formation during the electrospinning process. The PU/Col I yarns were obtained when the flow rates in the two syringes were 1.0 mL h^{-1}, the voltage was +10 kV and −10 kV, respectively. The distance of syringes to funnel was 15 ± 3 cm, with the angle between nozzles and the yarn being 45 ± 5°, and the rotating rate of the funnel was 400 rpm with a winding up speed of 1 m min^{-1}. The electrospinning process was terminated after 2 h. The structure and diameter of the resulting nanofibers and yarns were examined using scanning electron microscope (SEM), and their composition was confirmed by Fourier Transform Infrared Spectroscopy (FT-IR). In short, the sample was coated with Au/Pd using a Hummer 6 sputter (Anatech, CA, USA) and then imaged using a Hitachi 8230 cold Field-emission SEM (Tokyo, Japan). The average diameters and angle distribution (relative to the vertical axis) of the nanofibers were determined by analyzing 100

nanofibers in the SEM images using ImageJ software [27,30]. The contact angle was measured by a contact angle meter. We placed the yarn flat on the experimental table, and then dropped 5 μL of water on the surface of the yarn. Then the camera took pictures and recorded the contact angle. The mechanical properties of the yarns were tested by a mechanical testing machine.

The yarns' interaction with tendon derived stem cells (TDSCs) was evaluated by seeding cells on the scaffolds and assessing cell viability, morphology, and differentiation using various biochemical assays. The TDSCs were isolated as previous work [31] and subjected to corresponding experiments to evaluate the scaffolds' cytocompatibility. The scaffolds were affixed onto circular glass slides using biological adhesive and subsequently attached to a 24-well plate. The plain glass was utilized as the control group. Following a 6-h fumigation with 75 % alcohol and 0.5-h exposure to ultraviolet radiation, TDSCs were seeded onto the nanofiber scaffolds at a density of 1×10^4 cells per well for durations of 1, 3, 5, and 7 days. Subsequently, the cells were rinsed with PBS and fresh complete culture medium supplemented with a CCK-8 reagent (10 %) was added to each well. After incubation for 3 h, the plate was agitated for 15 min and the absorbance of the supernatant at a wavelength of 450 nm was quantified using a microplate reader. Immunofluorescence staining for F-actin/DAPI was conducted after a 3-day culture period, and cellular morphology was observed using a microscope. After culturing the TDSCs for 3 days, the culture medium was removed and samples were fixed with 3 % glutaraldehyde for 30 min at room temperature. Subsequently, permeabilization was achieved by treating the samples with 0.1 % Triton X-100 for 5 min, followed by three washes with PBS. Each sample was then incubated in a solution of bovine serum albumin (BSA) containing 0.1 % F-actin at room temperature in darkness for 30 min. Following three additional washes with PBS, mounting tablets containing DAPI were added to facilitate observation under an Olympus IX73 inverted microscope. The qRT-PCR assay was conducted to assess the expression of tenogenesis-related genes, including Scleraxis (SCX), Tenomodulin (TNMD), and Type I collagen (COL I), across different scaffold groups. The total RNAs were extracted from TDSCs using TRIzol reagent. The relative expression level of RNA was assessed by quantitative qRT-PCR, with the housekeeping gene glyceraldehyde-3-phosphate dehydrogenase (GAPDH) serving as the internal control. All PCR amplifications were conducted in a final reaction mixture volume of 20.0 μL, and the primer sequences used are provided in Table S1, supporting information. The amplification reaction was performed using ChamQ Universal SYBR qPCR Master Mix (Vazyme, Q711-02, China) for 40 cycles, and relative expression was calculated according to the $2^{-\Delta\Delta Ct}$ method.

2.3. Creation and assessment of PLLA/BG nanofiber membrane

Electrospinning synthesized the PLLA/BG nanofiber membrane similarly. Briefly, PLLA was dissolved in hexafluoroisopropanol at a concentration of 10 wt %, and the BG was directly mixed into the solution for electrospinning. In the electrospinning process, the solution was aspired into a 5-mL syringe, which was subsequently installed on the spinning equipment. The solution was pumped out at a rate of 1.0 mL h^{-1} through a blunt needle (22-gauge). A high voltage of 15 kV was applied between the needle and a grounded collector with 100 rpm speed separated by 15 cm. The electrospinning process was terminated after 1 h. The inclusion of BG into PLLA nanofibers aimed to enhance osteoconductive properties. The membrane's fiber diameter and morphology were characterized using SEM. The addition of BG was confirmed by transmission electron microscope (TEM). Similarly, the average diameters and angle distribution (relative to the vertical axis) of the nanofibers were determined by analyzing 100 nanofibers in the SEM images using ImageJ software. The contact angle was measured by the contact angle meter. The mechanical properties of the nanofiber membranes were tested by a mechanical testing machine.

The biocompatibility and osteogenic potential of the PLLA/BG membrane were assessed by culturing bone marrow mesenchymal stem cells (BMSCs) on the membrane and evaluating cell behavior, differentiation, and mineralization capabilities. The F-actin staining was conducted on BMSCs following co-cultivation with the PLLA/BG nanofiber membrane for a duration of 3 days. To determine the optimal concentration of BG, we fabricated PLLA/BG nanofiber membranes with varying BG concentrations (0 %, 1 %, 2 %, and 3 %). Subsequently, we conducted CCK-8 assays, ALP quantitative detection, and qRT-PCR experiments to evaluate these scaffolds' cell affinity and differentiation induction ability. The CCK-8 and qRT-PCR assays were conducted as described above. The expression of osteopontin (OPN), runt-related transcription factor 2 (RUNX2), and alkaline phosphatase (ALP) genes was assessed using qRT-PCR. ALP activity was quantified using the Alkaline Phosphatase Assay Kit E1040 after co-culturing BMSCs with PLLA/BG nanofiber membranes for 7 and 14 days.

2.4. Assembly of multi-layered scaffold

A multi-layered nanofiber-reinforced scaffold was constructed by strategically combining the acellular tendon, PU/Col I yarn, and PLLA/BG nanofiber membrane. The three-layer structure was assembled by fabricating and trimming the acellular tendon to the appropriate size and then wrapping PU/Col I yarn on its surface. Subsequently, both were fixed onto a specific electrospinning collection device and rotated to collect the PLLA/BG nanofiber membrane on the surface. The acellular tendon served as the central core, supplemented with PU/Col I yarn, and ultimately enveloped by PLLA/BG nanofibers. The PLLA/BG fibrous membrane was excised from the middle section of the scaffold, while silk sutures were employed to suture the ends of the scaffolds together. This scaffold aimed to replicate the complex hierarchical structure of the native tendon-bone interface. Each layer's integration and overall scaffold architecture were carefully examined to ensure structural integrity and functional efficacy.

2.5. Animal model and surgical procedure

The efficacy of the scaffold was tested in a rat ACL reconstruction model. Rats were divided into groups receiving the complex scaffold, acellular tendon, or control treatment. A total of 50 adult male Sprague Dawley rats (8 weeks old; weighing between 250 and 270 g) were randomly allocated into three groups: the Complexus group (n = 20), the acellular tendon (ATendon) group (n = 20), and the Control group (n = 10). The rats were anesthetized using a 4 % chloral hydrate solution at a dosage of 1 mL per 100 g of body weight. A standard medial parapatellar arthrotomy was performed to gain access to the right knee. The native ACL was identified and excised, followed by the anterior translation of the tibia to confirm complete resection of the ACL and visualize the tibial ACL footprint. The bone tunnels in the proximal tibia and distal femur were created using a 1.6 mm dental drill while maintaining extreme knee joint flexion. Subsequently, the composite scaffold or acellular tendon was threaded through these tunnels. The knee was then flexed to 30°, and both ends of the graft were sutured to the surrounding periosteum at the tunnel exit. The incisions were closed using sutures, and there were no postoperative restrictions on physical activity. The rats that underwent surgery were individually housed in unrestricted single cages, allowing for free movement. Graft healing was evaluated post-surgery through biomechanical testing, Micro-CT (SkyScan 1176; Bruker) imaging, and histological analyses. All animal experiments were approved by Qingdao University Laboratory Animal Welfare Ethics Committee (No.20210901SD6620231101129) as well as the ARRIVE Guidelines.

2.6. Comprehensive evaluation of scaffold performance

The right knee joint samples were harvested at weeks 4 and 8, while five samples of the left knee joint were collected as a normal group for

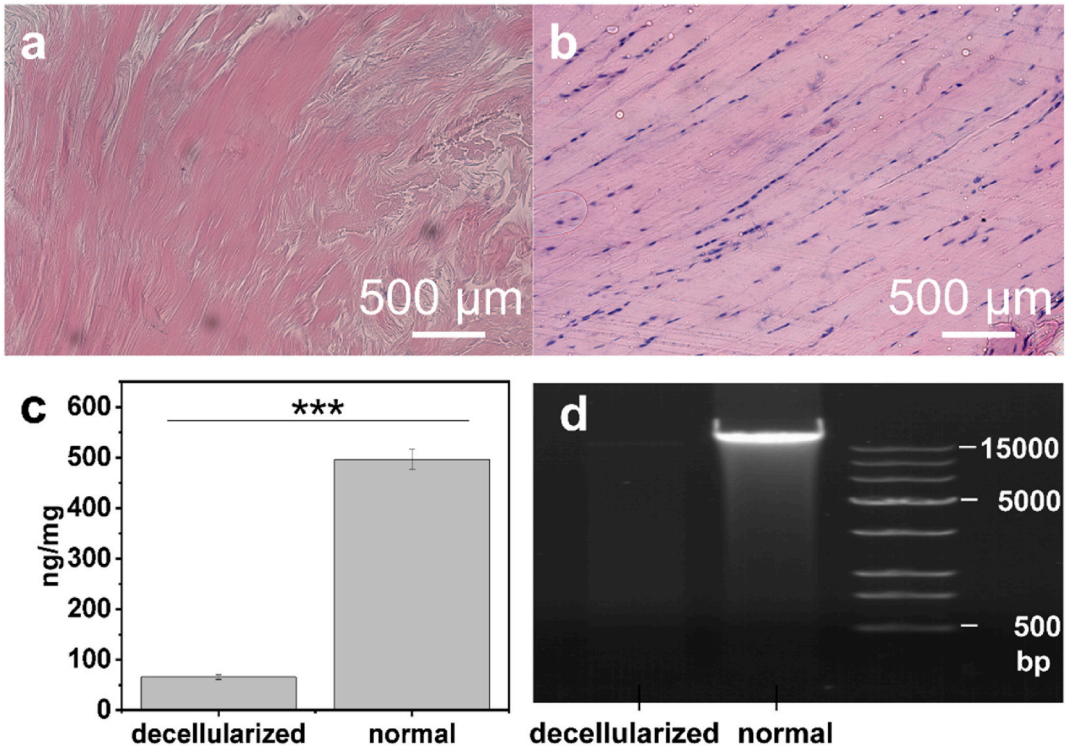

Fig. 1. Characterization of decellularized tendons and normal tendons. (a) Decellularized tendon H&E staining. (b) Normal tendon H&E staining. (c) Comparison of DNA content between decellularized tendons and normal tendons, (***$P < 0.001$). (d) The results of agarose gel electrophoresis.

biomechanical stress experiments. Five samples from each time point were utilized for biomechanical testing, and an additional five samples were used for Micro-CT detection. Subsequently, the specimens underwent fixation, decalcification, embedding, and sectioning before being subjected to observation through H&E and Masson (Solarbio) staining. The biomechanical strength of the reconstructed ACLs was assessed using a biomechanical testing machine. Briefly, the tibia and femur were securely fastened using two clamps to ensure that the applied load was effectively aligned with the longitudinal axis of the graft. The ultimate failure load and Young's modulus were measured at an extension velocity of 0.25 mm/s. The mode of graft failure was documented as either a pullout from the bone tunnel or a rupture of the intermediate material. Throughout the experiment, samples were maintained in a moist environment using a saline solution.

Micro-CT imaging provided insights into new bone formation, while histological analyses (H&E and Masson staining) revealed the quality of tissue integration and healing. Micro-CT scanning and evaluations of the samples, collected at 4 and 8 weeks after surgery, were performed. The scanning parameters employed were as follows: a source voltage of 65 kV, a source current of 385 mA, an image rotation of 0.1840, and an aluminum filter thickness of 1 mm. The scanned sections were reconstructed in three dimensions and subsequently rotated using NRecon software (Version 1.7.0.4; Bruker) to achieve vertical alignment of the bone tunnel. The image data were analyzed using Analyzer software (Version 1.8.1.3; Bruker). The volume of interest for new bone formation within the tibial and femoral bone tunnels was defined as a cylindrical region with a diameter of 1.6 mm and a height spanning 50 slices. The evaluation of new bone formation in the bone tunnel and surrounding bone changes after surgery was based on the ratio of bone volume to total volume (BV/TV).

After undergoing Micro-CT scanning, the samples were subsequently fixed using paraformaldehyde, decalcified utilizing an EDTA solution, and finally embedded in paraffin. The embedded samples were sectioned perpendicularly to the longitudinal axis of the bone tunnel at a thickness of 5 μm. H&E, Masson, and immunohistochemical staining for COL I and SCX were performed following standard protocols, and the specimen sections were observed using an inverted microscope to capture images. In order to observe the role of osteoclasts in the healing process, tartrate resistant acid phosphatase (TRAP) staining was performed with a commercial TRAP staining kit (G1050, Ser-vicebio, China) according to the manufacturer's instructions. Immunofluorescence staining for Tenascin C (TNC) and Osteocalcin (OCN) was performed as described earlier to analyze the expression levels of tendon-related and bone-related proteins in reconstruction part. Briefly, the sections were deparaffined, hydrated, inactivated with endogenous peroxidase, repaired with antigens, blocked with 5 % normal goat serum, and then incubated overnight at 4 °C using TNC (rabbit anti-rat 1:500) or OCN (rabbit anti-rat 1:500) monoclonal antibodies, followed by incubation with goat anti-rabbit 594 conjugated secondary antibody (1:500) and goat anti-rabbit 488 conjugated secondary antibody (1:500) for 1 h. The sections were mounted using mounting tablets containing DAPI and examined under an immunofluorescence microscope (Nikon).

2.7. Statistical methods

Statistical analyses were conducted using one-way ANOVA and students' t-tests to compare the outcomes among different groups. The results were reported as mean ± standard deviation, ensuring the rigor and reliability of the data.

3. Results and discussion

3.1. Acellular tendon generation

Fig. 1 demonstrates the successful decellularization of tendons. After decellularization, nuclei in tendon tissue disappeared. (Fig. 1a and b). The significant reduction in DNA content post-decellularization (496.53 ± 19.69 ng/mg to 65.52 ± 4.30 ng/mg) and the absence of DNA bands in agarose gel electrophoresis confirms the effective removal of cellular material. The observed disparity between the two groups exhibited

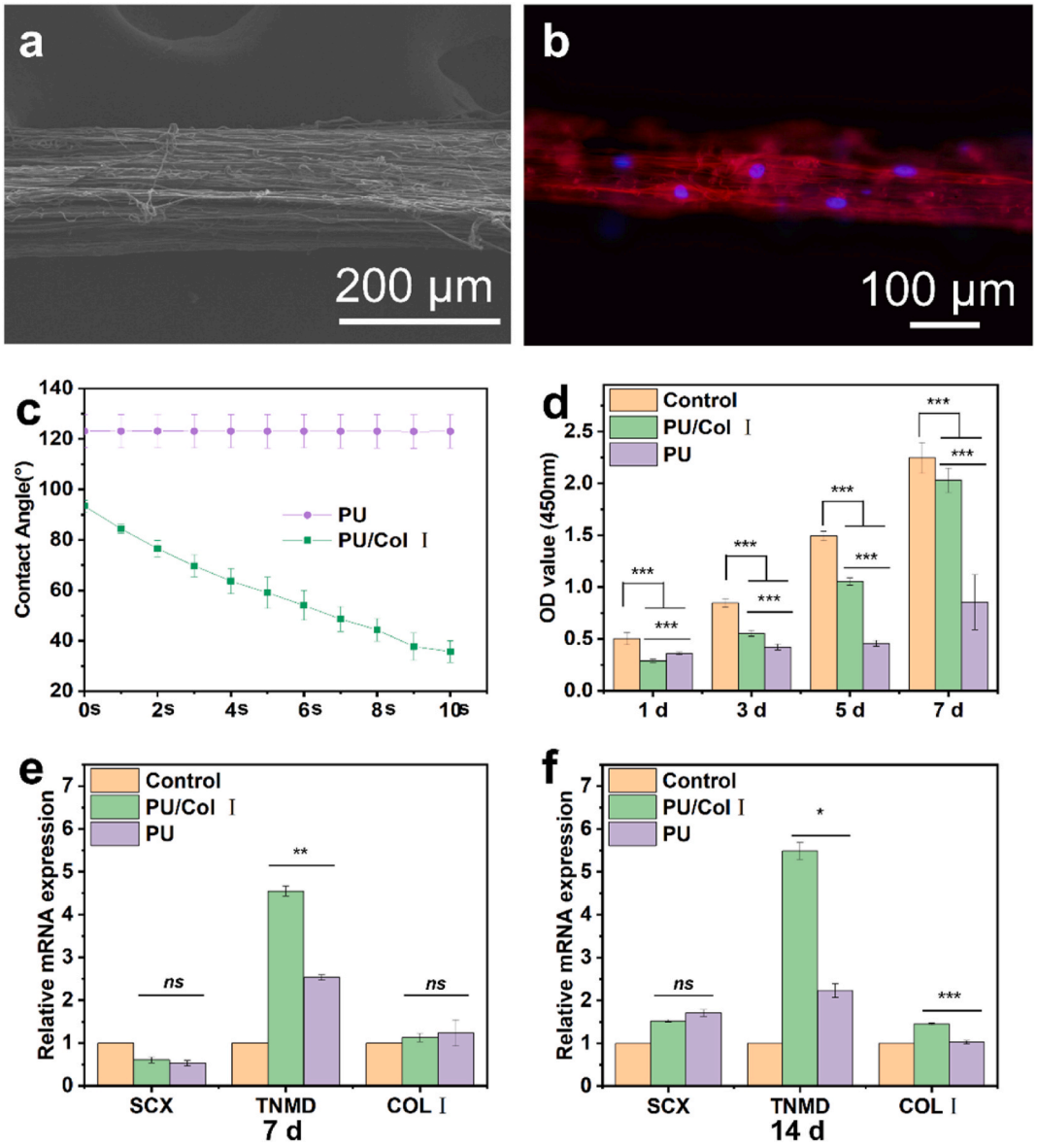

Fig. 2. Characterization of PU/Col I yarn. (a) The SEM images of PU/Col I yarn. (b) Fluorescence micrographs showing the morphologies of TDSCs after co-culturing with the PU/Col I yarn for 3 days. The cells demonstrate a morphology characterized by elongation. (c) The contact angle of PU yarn and PU/Col I yarn. The contact angle of the PU yarn remained consistently stable at 123° ± 7°, while the angle of PU/Col I yarn was significantly decreased to 36° ± 6° within 10 s. (d) The proliferation of TDSCs on the different samples tested by CCK-8 assay on days 1, 3, 5, and 7. The addition of Col I enhances the cell proliferation of yarn. (e, f) qRT-PCR results detecting the tendinogenesis-related genes (SCX, TNMD, and COL I) expression of TDSCs cultured with different samples. The addition of Col I enhances the expression of TNMD and COL I. (*$P < 0.05$, **$P < 0.01$, ***$P < 0.001$).

statistical significance ($P < 0.001$) (Fig. 1c). DNA agarose gel electrophoresis revealed the presence of whole-genome DNA bands in the fresh tendon group, whereas no discernible DNA bands were observed in the acellular tendon group (Fig. 1d). Decellularized tendons comprise extracellular macromolecules such as collagen, elastin, fibronectin, laminin, and matrix cell proteins [32]. The structure and composition are highly similar to natural tissues, providing an ideal three-dimensional environment for tissue regeneration. By removing immunogenic cellular components, the risk of rejection is minimized. This approach exhibits excellent potential and advantages [33]. These acellular tendons, retaining key extracellular macromolecules such as collagen and elastin, provide an immunogenically inert yet structurally appropriate scaffold for tissue regeneration.

3.2. Biocompatibility and differentiation potential of PU-Col I yarn on TDSCs

PU yarn embedded with Col I was successfully developed, exhibiting a parallel nanofiber arrangement (Fig. 2a). The yarn structure closely resembles the natural tendon's hierarchical arrangement, enhancing tensile strength [34–36]. The yarn's similarity to collagen fibers in tendons (Fig. S1a, Supporting Information) and the presence of Col I (confirmed by FT-IR analysis, Fig. S1b, Supporting Information) emphasize its biomimetic properties. Pure collagen contained the absorption peak at 1653 cm^{-1}, corresponding to amide I [27]. In our experiment, the yarns made by PU and Col I showed such absorption peaks at 1653 cm^{-1}, thus indicating the successful addition of Col I. Manipulation of production parameters enables precise adjustment of yarn diameter and width [37]. The diameter of the yarns was 107.96 ± 23.67 μm, and the diameter of these nanofibers measures 859.44 ±

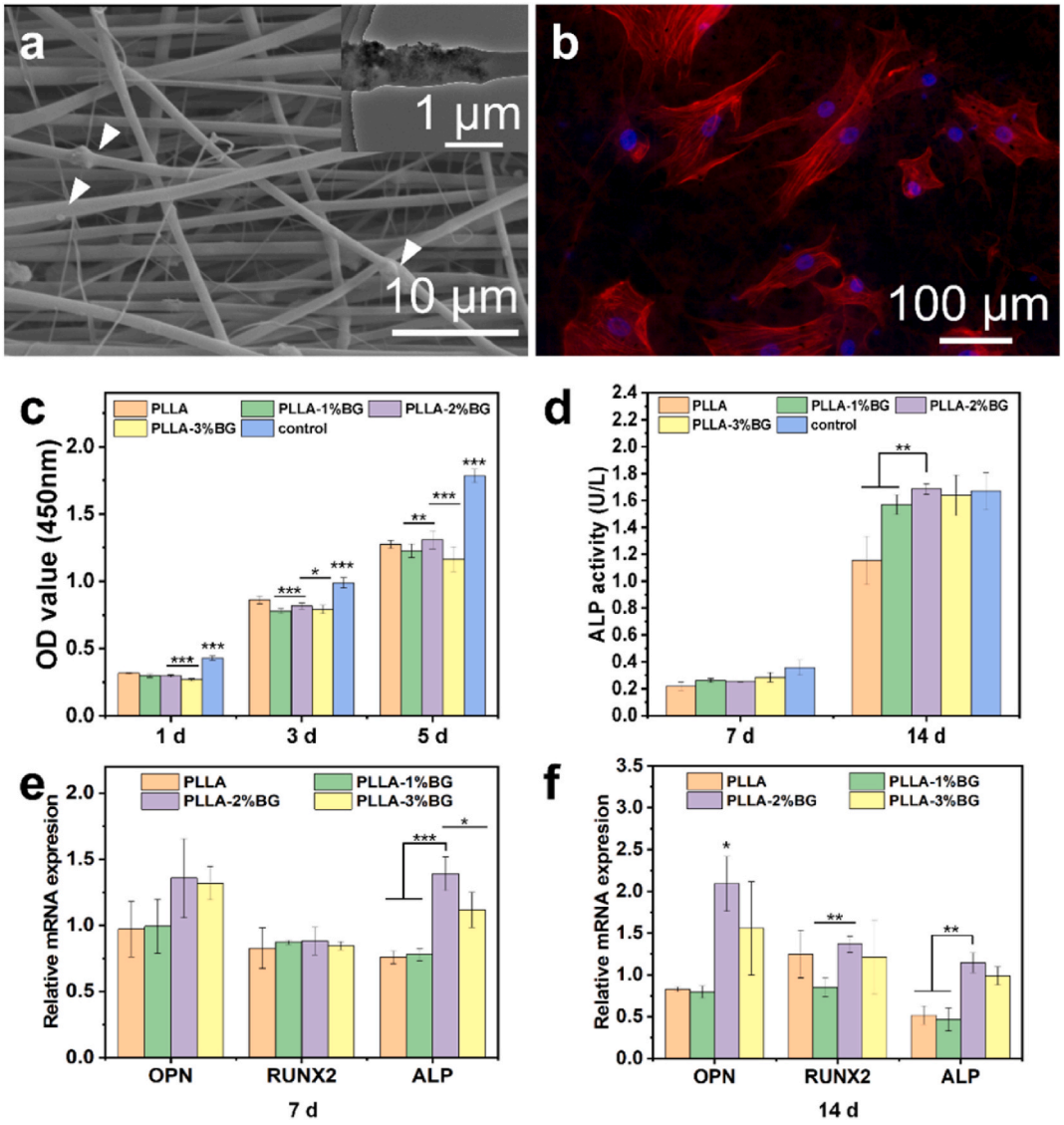

Fig. 3. Characterization of PLLA/BG nanofiber membrane. (a) The SEM and TEM images of PLLA/BG nanofiber membrane. (b) Fluorescence micrographs showing the morphologies of BMSCs after co-culturing with the PLLA/BG nanofiber membrane for 3 days. The cells were spread on the membrane. (c) The proliferation of BMSCs on the different samples tested by CCK-8 assay on days 1, 3, and 5. The proliferation of BMSCs seeded on the membrane with a 2 % concentration of BG is better than that on the membranes with 1 % and 3 % concentration of BG on days 3 and 5. The membrane with a 2 % concentration of BG exhibits the most pronounced enhancement in cell proliferation. (d) Quantitative analysis of APL shows the expression of ALP in the different groups. The 2 % concentration of BG demonstrates a superior effect in promoting ALP expression compared to concentrations of 0 % and 1 % BG. (e, f) qRT-PCR results detecting the osteogenic gene (ALP, RUNX2, and OPN) expression of BMSCs cultured with different PLLA/BG nanofiber membranes containing different BG concentrations. The 2 % concentration of BG demonstrates remarkable efficacy in promoting the expression of osteogenic genes in BMSCs. (*$P < 0.05$, **$P < 0.01$, ***$P < 0.001$).

149.24 nm, which is comparable to the range of collagen fibers found in tendons (from a few nanometers to 500 nm). The nanofibers in the yarns mainly formed angles ranging from 80° to 90° (Fig. S1c, Supporting Information). In the mechanical test, the ultimate failure load and Young's modulus of the PU yarn and PU/Col I yarn did not have significant differences (Figs. S1d and e, Supporting Information). However, one distinguishing feature lies in the absence of an enveloping sheath composed of connective tissue around the yarns. Nevertheless, this characteristic also facilitates cell infiltration due to increased available space. The primary physiological function of ACL cells is to secrete type I and type III collagen proteins, which subsequently undergo interconnection to form dense collagen fibers [38]. The natural tendons and ligaments are composed of cross-linked Col I and human type I, and III collagens, which are the primary constituents of the anterior cruciate ligament [39]. Collagen-based scaffolds are extensively utilized for promoting the repair of tendons and ligaments due to their predominant composition of Col I, which confers inherent biocompatibility [40,41]. The inoculation of TDSCs onto the surface of the yarn resulted in the observation of an elongated and longitudinally aligned morphology of the cells along the yarn (Fig. 2b). Without Col I, the contact angle of PU yarn is 123° ± 7°. However, upon incorporating Col I, there was a significant decrease in contact angle to 36° ± 6° within 10 s (Fig. 2c, Fig. S1f, Supporting Information). This enhanced hydrophilicity and the yarn's structural properties contributed to increased TDSCs proliferation and tendon-like differentiation (Fig. 2d–f). Compared to PU yarn, incorporating Col I in the PU yarn significantly enhanced cell proliferation at 3, 5, and 7 days. The observed phenomenon may be attributed to the incorporation of the tendon component Col I [27]; alternatively, it could be ascribed to the enhanced hydrophilicity of the fibrous membrane following Col I addition. The qRT-PCR analysis revealed that, on the 7th day, PU/Col I yarn significantly upregulated the expression of TNMD in TDSCs. Furthermore, on the 14th day, it notably enhanced the

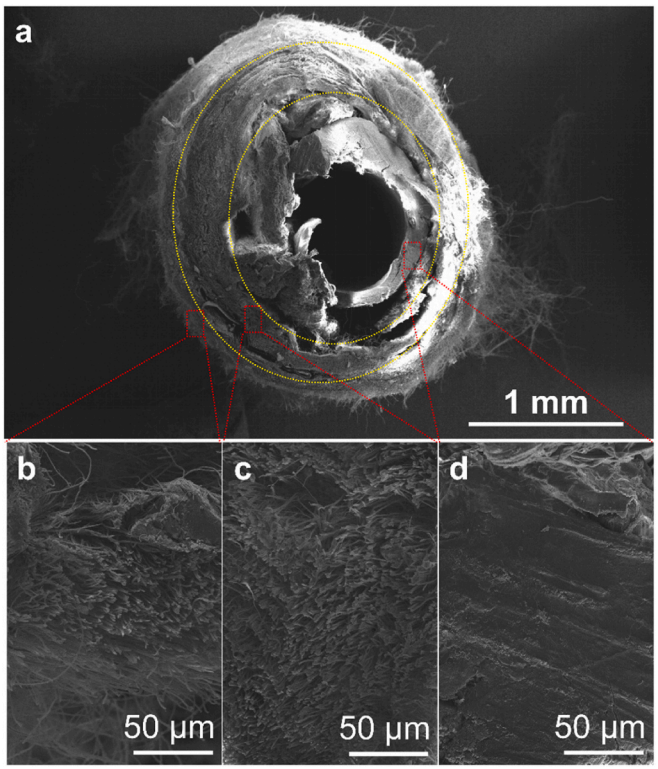

Fig. 4. The SEM images of multi-layer nanofiber-reinforced three-dimensional scaffold for acellular tendon complex. (a) The SEM image of a cross section of tendon complexus. (b) The SEM image of cross section of the PLLA/BG nanofiber membrane. (c) The SEM image of a cross section of PU/Col I yarn. (d) The SEM image of a cross section of the acellular tendon.

expression of TNMD and COL I genes. This suggests that yarn containing Col I can induce tendon-like differentiation of TDSCs. The capacity for promoting differentiation may be attributed to the organized arrangement of yarn structure and the presence of ECM Col I within the yarn.

3.3. Biocompatibility and differentiation potential of PLLA/BG nanofiber membranes on BMSCs

The PLLA/BG nanofiber membrane, with successfully incorporated BG (Fig. 3a), exhibited optimal biocompatibility and osteogenic potential at a 2 % BG concentration. Various assays, including CCK-8 and qRT-PCR, demonstrated this, indicating the membrane's ability to induce BMSCs differentiation towards osteogenic lineages (Fig. 3c–f). By observing the SEM and TEM images, it was found that BG had been successfully incorporated. The average diameter of PLLA/BG nanofibers was 902.2 ± 172.1 nm (Fig. S2a, Supporting Information). The nanofibers in the random scaffold exhibited equal distribution at all angles (Fig. S2b, Supporting Information). The contact angle was similar in PLLA nanofiber membranes with different BG contents (Fig. S2c, Supporting Information). In the mechanical test, the ultimate failure load and Young's modulus of the PLLA nanofiber membranes containing different BG content did not have significant differences (Figs. S2d and e, Supporting Information). The BMSCs were isolated and characterized (Fig. S3, Supporting Information). The observation of BMSCs seeded on the nanofiber membrane revealed a diverse range of cellular morphologies (Fig. 3b). When BG is exposed to body fluids, ions such as Si, Ca, and P are rapidly released from the BG and form a hydroxyapatite layer on the surface [42], thereby inducing cell differentiation and promoting bone regeneration. The PLA scaffold exhibits a strong affinity towards cells, which the addition of fibronectin can further augment [43]. We fabricated samples with varying concentrations of 0 %, 1 %, 2 %, and 3 % BG to determine the optimal BG content in the nanofiber membranes, followed by conducting corresponding cellular experiments. Based on the CCK-8 experiment, nanofiber membranes with a 2 % BG concentration exhibited significantly higher results on the 3rd and 5th days compared to concentrations of 1 % and 3 %. In order to investigate the impact of BG addition on BMSCs differentiation, we performed ALP activity and qRT-PCR assays. The results from the ALP activity test demonstrated that, on day 14, a 2 % concentration of BG significantly enhanced ALP expression in BMSCs compared to nanofiber membranes with 0 % and 1 % BG content. The qRT-PCR experiment further confirmed this finding. Specifically, on the 7th day, the nanofiber membrane containing 2 % BG notably upregulated ALP gene expression in BMSCs. Moreover, on the 14th day, the nanofiber membrane with a concentration of 2 % BG promoted OPN, RUNX2, and ALP gene expression in BMSCs. Therefore, the PLLA nanofiber membrane containing 2 % BG content demonstrates optimal cellular affinity and osteogenic potential for inducing BMSCs differentiation towards bone formation. Consequently, this membrane can be employed as the outer layer of a composite scaffold to effectively enhance bone regeneration.

3.4. Multi-layer nanofiber-reinforced scaffold fabrication

The scaffold must be meticulously designed with characteristics appropriate for its intended function, and its surface morphology must be precisely tailored to facilitate cell attachment and differentiation [44]. By controlling the structural and biochemical cues of fibers, cell behavior in tissue repair can be regulated [45,46]. The multi-layer scaffold was successfully fabricated, combining a decellularized tendon core, a PU/Col I yarn middle layer, and an outer PLLA/BG nanofiber membrane (Fig. 4 and S4a, Supporting Information). The thickness of the middle layer (PU/Col I yarn) was 327.01 ± 65.21 μm, and the out layer (PLLA/BG nanofibers) was 97.47 ± 6.43 μm. This scaffold mimics the natural tendon-to-bone interface in structure and composition, potentially enhancing tendon-bone healing. The hollow section is formed after removing the metal rod utilized for receiving the outer layer in the previous step. It will be joined together using a suture thread during subsequent fabrication processes. The length of the scaffolds measured approximately 1 cm. Tang et al. designed a biphasic electrospinning scaffold with randomly arranged phases at both ends and an aligned phase in the middle. They validated through *in vitro* experiments that different fiber structures promote differences in cellular morphology and induce fibroblast differentiation during dynamic cultivation [47]. In comparison, the yarn structure used in this study exhibits better orientation and provides more ample spatial structure, facilitating cell infiltration [23]. Caroline et al. utilized the three-dimensional hexagonal weaving technique to fabricate a polydioxanone scaffold as an alternative for the ACL [48]. Their findings revealed that the woven scaffold demonstrates superior tensile strength compared to the natural ACL. However, no relevant *in vivo* or *in vitro* experiments have been conducted. Silk collagen scaffolds modified with hydroxyapatite at both ends have been used to reconstruct the ACL. In *in vivo* experiments, a large amount of mature bone formation was observed in the tendon-bone interface, and more Col I and osteocalcin deposition were observed in immunohistochemical staining [49]. Zhang et al. employed a layer-by-layer self-assembly method to fabricate a multi-functional hybrid ligament by combining degradable and non-degradable stents. They prepared a poly (caprolactone) nanofiber membrane loaded with BMP 7 as the degradable component of the mixed ligament. Subsequently, this nanofiber membrane was rolled with a poly (ethylene terephthalate) mesh (non-degradable component), forming a 'Swiss roll' structure [50]. The layered structure of the complex tendon exhibits greater distinctiveness in comparison. In order to combine the layers closely, photothermal welding can partially melt the scaffold and weld it together, which provides some ideas for future research [51,52]. The complex tendon has a more fitting biomimetic structure, with the outer layer simulating the random structure and components of bone ends, the middle layer mimicking the orientation

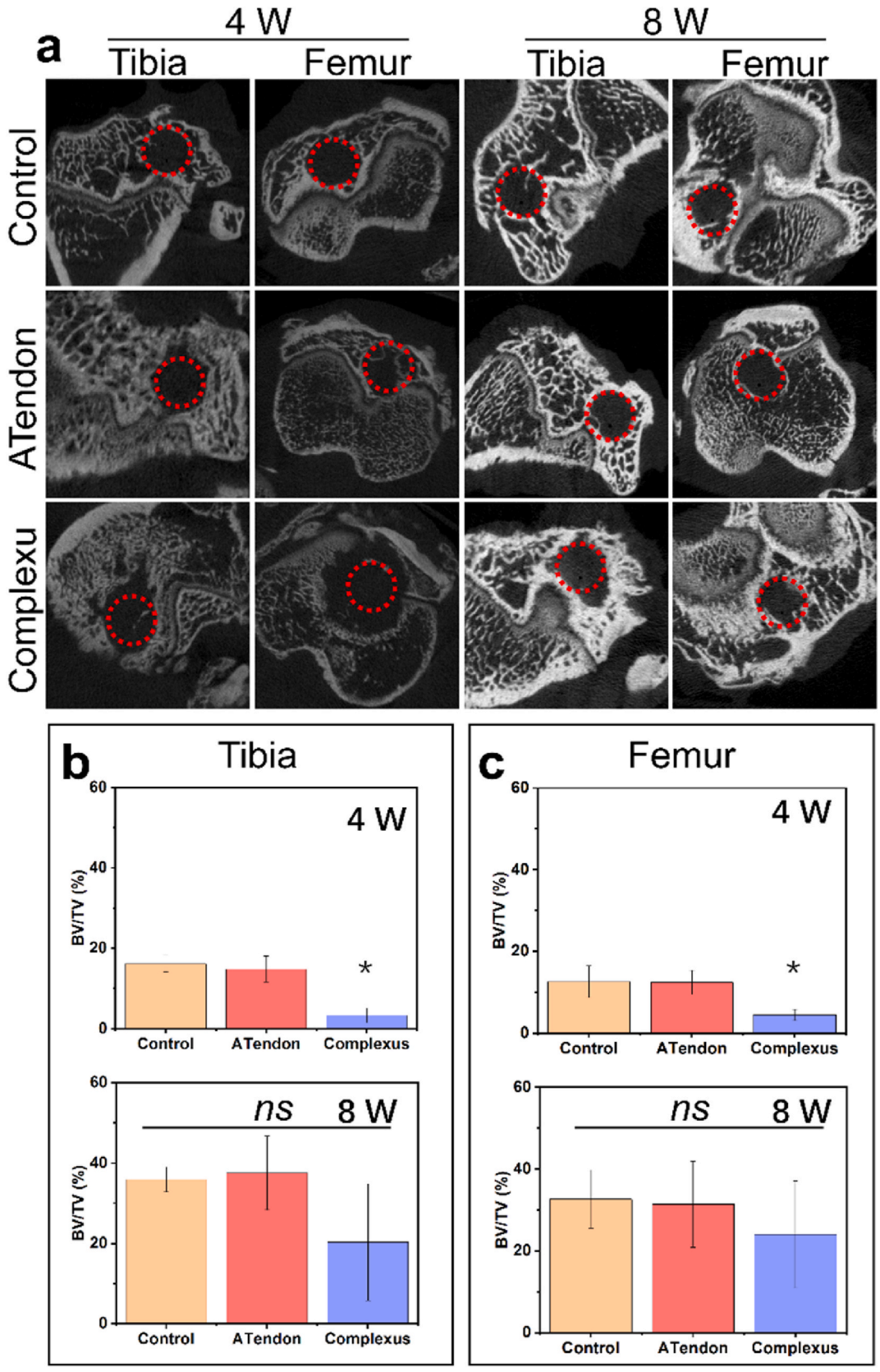

Fig. 5. The images and analysis of Micro-CT test in different groups at 4 and 8 weeks. (a) The images of Micro-CT test in different groups at 4 and 8 weeks. (b, c) Bone regeneration of bone tunnel in tibia and femur. $^{*}P < 0.05$ relative to the Control and ATendon groups. They show that the Complexus group has a significant difference with the Control group and ATendon group in bone regeneration of the tibia and femur at 4 weeks, but there is no significant difference in BV/TV results of tibia and femur at 8 weeks. ($^{*}P < 0.05$).

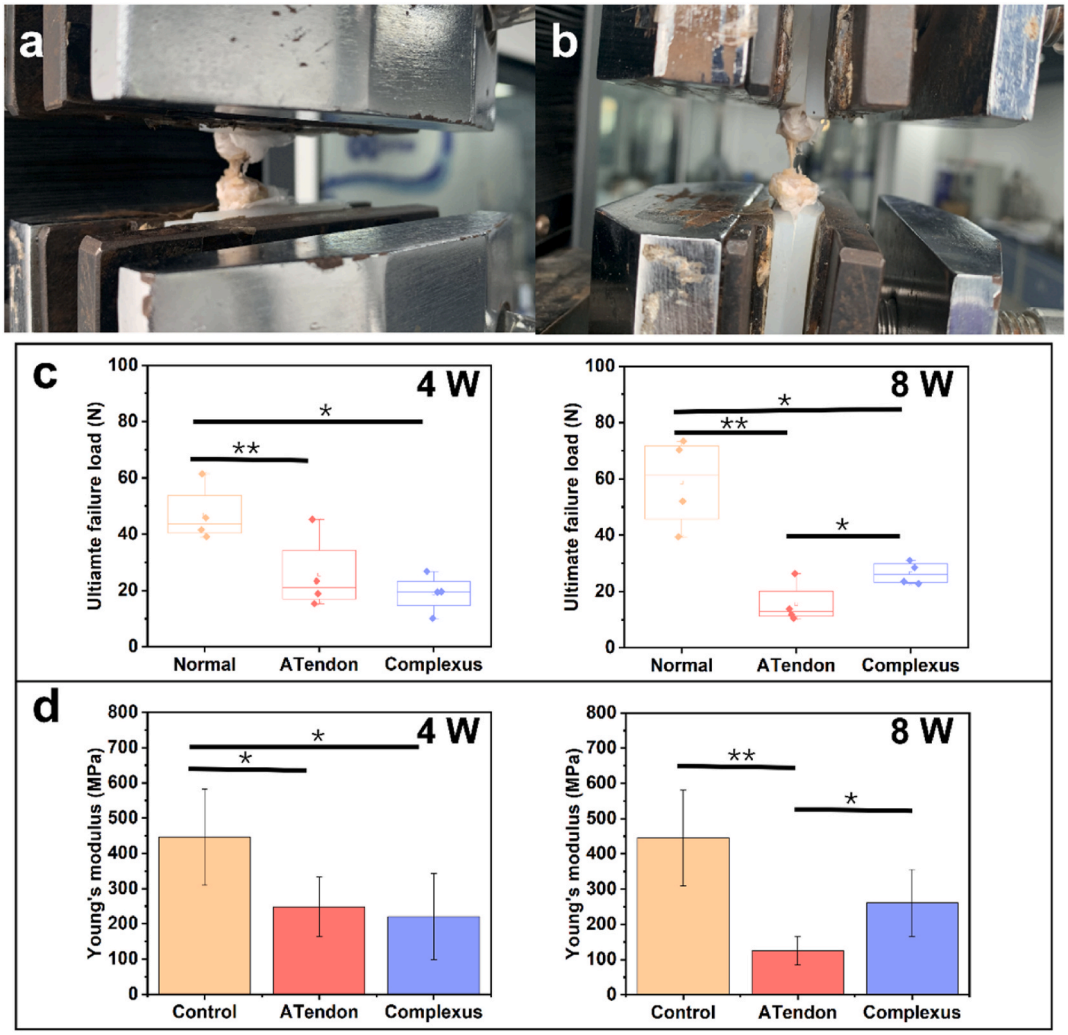

Fig. 6. Biomechanical tests of the scaffolds at 4- and 8-week post *in-vivo* implantation. (a, b) Photographs showing the biomechanical test procedure of the samples explanted at 4 or 8 weeks. (c) Ultimate failure load of the different samples. (d) Young's modulus of the different samples. (*$P < 0.05$, **$P < 0.01$).

structure and components of tendons, and the inner layer providing strong tensile strength and ECM components through decellularized tendons. The different degree of fiber orientation is obtained in concentric layers, rather than in different regions of the scaffold. Initially, we fixed each layer of the scaffold with surgical sutures. During the process of healing, the layers gradually integrate into a whole part with tissue filling, bone integration, and tendon regeneration, and finally achieve strong tendon-to-bone healing.

3.5. Animal experiment results

In vivo, evaluation in the rat's ACL reconstruction models revealed positive outcomes. The composite scaffold facilitated better integration and mechanical properties compared to controls. Macroscopic examination revealed intact grafts within the knee joints without any signs of fractures, but evidence of cartilage detachment on the joint surface was observed (Figs. S4c–h, Supporting Information). However, there was an initial reduction in bone mass in the Complexus group, likely due to PLLA degradation byproducts, which resolved over time. The Micro-CT examination revealed a significantly lower bone mass within the Complexus group's tibial and femoral tunnels than the control and ATendon groups. This phenomenon may be related to the acidic byproduct of lactic acid produced after PLLA degradation, as lactic acid can induce mild aseptic inflammation [53,54]. Aseptic inflammation leads to bone resorption, resulting in the absence of bones detected by Micro-CT. Additionally, the enlargement of the bone tunnel may be attributed to the fixation method employed during the reconstruction process. During the operation, the graft and periosteum are fixed by needle and thread, which may result in transverse graft movement (windshield-wiper effect) and longitudinal graft movement (bungee effect) [55]. These movements can cause the enlargement of the bone tunnel. By the 8th week, there was no significant difference in bone mass among the three groups within the tunnels (Fig. 5). At 4 weeks post-implantation, many osteoclasts appeared in both the ATendon group and the Complexus group, and these osteoclasts were not observed at 8 weeks (Fig. S5, Supporting Information). This suggests that the enlargement of the bone tunnel in the Complexus group is associated with osteoclasts. In addition, the generation of osteoclasts may also be associated with the reaction between the body and materials, and the polarization of macrophages, which jointly participate in the process of bone regeneration [56]. The biomechanical testing results revealed no significant disparity in ultimate stress and Young's modulus between the ATendon group and the Complexus group at 4 weeks. However, at 8 weeks, the Complexus group demonstrated a significantly higher level of ultimate stress than the ATendon group, accounting only for 45.02 % of that observed in normal samples (Fig. 6c). In addition, Young's modulus of the ATendon group was significantly lower than that of the Complexus group at 8 weeks (Fig. 6d). The H&E staining confirmed the presence of well-structured soft tissue within the control tunnels, characterized by clearly defined bony edges, thus validating their integrity. Additionally,

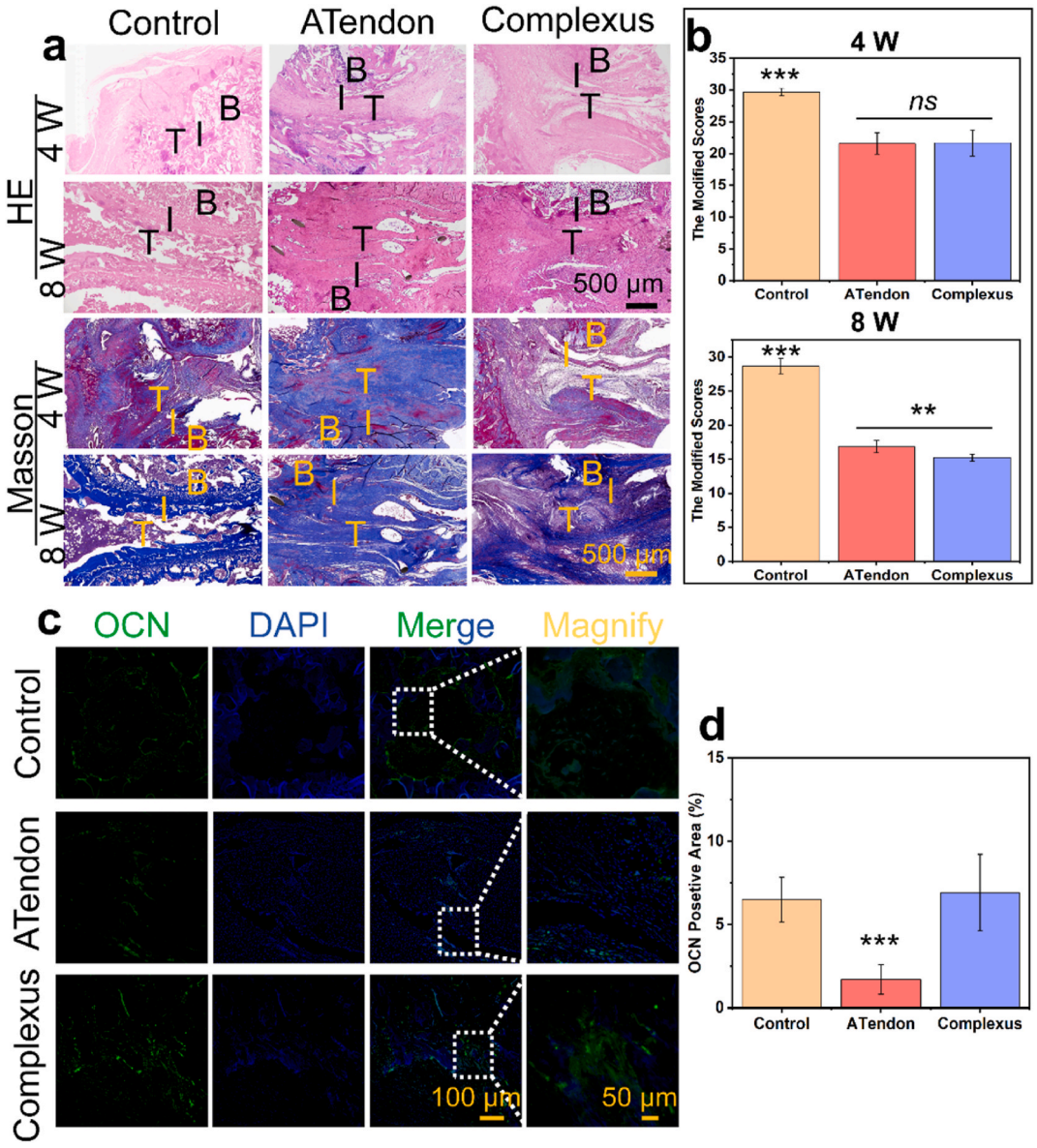

Fig. 7. H&E, Masson and immunofluorescence staining of the samples. (a) H&E and Masson staining of the samples. The Control group exhibited the formation of a robust osseous tunnel, while both the decellularized tendon group and Complexus group demonstrated successful integration of the graft with the surrounding bone tissue. (b) The modified tendon-to-bone maturity score of H&E and Masson staining. ***$P < 0.001$ as compared with the ATendon and Conplexus groups. The Complexus group resulted in a more mature attachment at 8 weeks of healing compared with ATendon group. (c) Immunofluorescence staining for OCN of the samples at 8 weeks. (d) Semi-quantitative analysis of immunofluorescence staining for OCN. ***$P < 0.001$ relative to the Control and Complexus groups. The Complexus group and Control group express more OCN protein than the ATendon group. (B: bone; I: interface; T: tendon; **$P < 0.01$, ***$P < 0.001$).

it revealed a distinct demarcation between decellularized tendons and surrounding bone, ensuring a secure attachment. Furthermore, the seamless integration of decellularized tendons, suture threads, and bone tissues was observed in the Complexus group. Masson staining demonstrated evident incorporation of colored substances within suture threads, potentially indicating ongoing tendon repair processes (Fig. 7a). The staining sections were semi-quantitatively analyzed by a blinded observer using a modified tendon-to-bone maturity score adapted from Shah et al. [57]. There was no significant difference in the scores between the ATendon group and the Complexus group at 4 weeks. At 8 weeks, the scores of the Complexus group were better than the ATendon group (Fig. 7b and Table S2, Supporting Information). This suggests that the complexus has a positive effect on tendon-to-bone healing. In immunofluorescence, more bone-related OCN protein was observed in the tendon-bone junction of the Complexus group than in the ATendon group (Fig. 7c and d). These results indicate that the PLLA/BG fibrous membrane contributes to the process of bone regeneration. OCN is an important protein for osteogenesis, and its expression reflects the activity of osteogenesis [58]. By observing immunohistochemical staining, the injured site in the Complexus group expressed more COL I than the ATendon group and the Control group at both 4 and 8 weeks (Fig. 8a and b). The expression COL I is critical in maintaining the tendon structure and function, consistent with the natural healing process of the tendon [59]. It was observed that there was more tendon-related protein expression (SCX and TNC) in the Complexus group in the immunohistochemical and immunofluorescence staining (Fig. 8c, d and Fig. S6, Supporting Information). TNC and SCX are the landmark factors for tendonogenic differentiation [60]. This suggests that the oriented structure of the yarn contributes to regular cell alignment and tendon-related protein production. A limitation of such a class of complexus is the enlargement of the bone tunnel at an early stage. The focus of future research will be on overcoming this problem. In

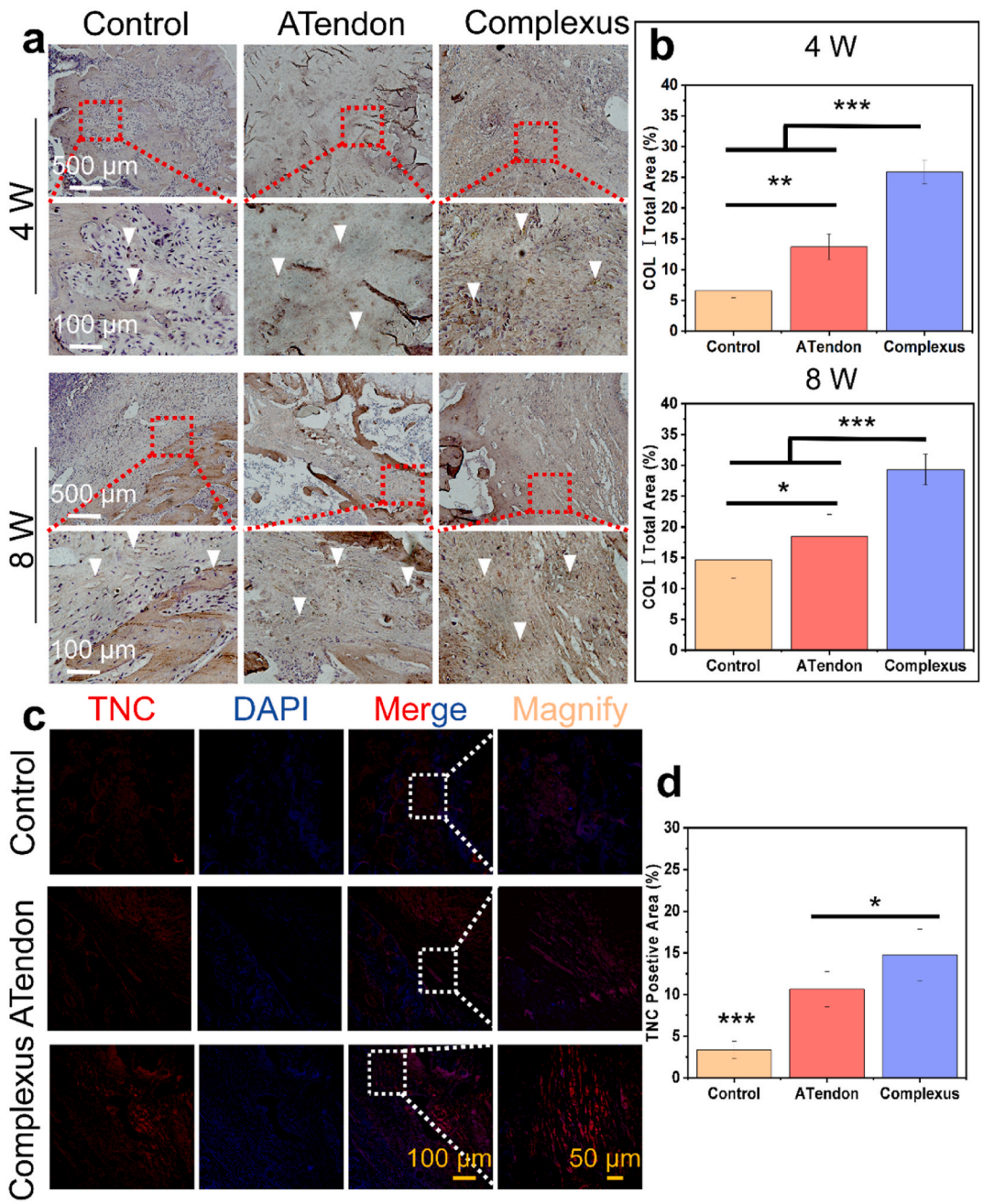

Fig. 8. Immunohistochemical and immunofluorescent staining of the samples and semi-quantitative analysis. (a) Immunohistochemistry staining of samples for type I collagen (COL I). (b) Semi-quantitative analysis of Immunohistochemistry staining for COL I. The Complexus group expresses more COL I than the ATendon group and Control group. (c) Immunofluorescence staining for TNC of the samples at 8 weeks. (d) Semi-quantitative analysis of immunofluorescence staining for TNC. ***$P < 0.001$ as compared with the ATendon and Conplexus groups. The Complexus group expresses more TNC protein than the ATendon group and Control group. (*$P < 0.05$, **$P < 0.01$, ***$P < 0.001$).

conclusion, the complexus are located at the junction of tendon-to-bone, and the oriented yarn can induce regular cell arrangement and promote the expression of tendon-related factors and proteins, and the random PLLA/BG nanofiber membrane could promote the expression of osteogenic factors and proteins, and ultimately promote the high-quality healing of tendon-to-bone interface.

4. Conclusion

The study introduces a novel multi-layer nanofiber-reinforced scaffold, showcasing its potential in ACL reconstruction. The scaffold's layers, each with specific properties, collectively contribute to an environment conducive to tissue regeneration and integration. Its overall structure consists of an inner layer composed of the decellularized tendon, which provides mechanical solid strength and ECM for the entire scaffold, facilitating immediate fixation of the composite structure and cell infiltration during healing; a middle layer with yarn that enhances overall strength, containing Col I fibers arranged in a three-dimensional and oriented manner to induce regular alignment of cells and their differentiation into tendon cells; an outer layer encapsulated by a randomly electrospun membrane, which contains BG and possesses random fiber arrangement, capable of inducing BMSCs to express osteogenic-related genes OPN, RUNX2, and ALP. Particularly in a rat anterior cruciate ligament reconstruction model, this composite scaffold

demonstrates excellent performance in enhancing integration between transplants and bone tissue as well as improving mechanical properties. Despite promising results, the rat ACL model's limitations highlight the need for extended *in vivo* studies to understand the scaffold's long-term performance fully. This scaffold represents a significant advancement in ACL reconstruction techniques, with potential applications in human orthopedic surgery.

CRediT authorship contribution statement

Chenghao Yu: Writing – review & editing, Writing – original draft, Visualization, Validation, Methodology, Formal analysis, Data curation, Conceptualization. **Renjie Chen:** Formal analysis, Data curation. **Jinli Chen:** Data curation, Conceptualization. **Tianrui Wang:** Methodology, Investigation, Formal analysis. **Yawen Wang:** Methodology, Investigation. **Xiaopei Zhang:** Methodology, Investigation. **Yuanfei Wang:** Project administration, Investigation. **Tong Wu:** Writing – review & editing, Supervision, Methodology, Investigation, Funding acquisition, Data curation, Conceptualization. **Tengbo Yu:** Writing – review & editing, Supervision, Project administration, Investigation, Funding acquisition.

Declaration of competing interest

The authors declare that they have no known competing financial interests or personal relationships that could have appeared to influence the work reported in this paper.

Data availability

Data will be made available on request.

Acknowledgements

This research was supported by Key Research and Development Program of Shandong Province (2021SFGC0502), Natural Science Foundation of Shandong Province (ZR2021YQ17), the Special Funds for Taishan Scholars Project of Shandong Province (No. tsqn202211125), Young Elite Scientists Sponsorship Program by China Association for Science and Technology (No. YESS20200097). The authors also thank the "Advanced Biomaterials and Regenerative Medicine (ABRM)" Innovation Team supported by the Young-Talent Introduction and Cultivation Plan in the Universities of Shandong Province.

Appendix A. Supplementary data

Supplementary data to this article can be found online at https://doi.org/10.1016/j.mtbio.2024.101099.

References

[1] K.E. Webster, Return to sport and reinjury rates in elite female athletes after anterior cruciate ligament rupture, Sports Med. 51 (4) (2021) 653–660.
[2] B. Moses, J. Orchard, J. Orchard, Systematic review: annual incidence of ACL injury and surgery in various populations, Res. Sports Med. 20 (3) (2012) 157–179.
[3] Q. Jiang, L. Wang, Z. Liu, et al., Canine ACL reconstruction with an injectable hydroxyapatite/collagen paste for accelerated healing of tendon-bone interface, Bioact. Mater. 20 (2023) 1–15.
[4] J. Cai, Q. Zhang, J. Chen, et al., Electrodeposition of calcium phosphate onto polyethylene terephthalate artificial ligament enhances graft-bone integration after anterior cruciate ligament reconstruction, Bioact. Mater. 6 (3) (2020) 783–793.
[5] M.W. DeFazio, E.J. Curry, M.J. Gustin, et al., Return to sport after ACL reconstruction with a BTB versus hamstring tendon autograft: a systematic review and meta-analysis, Orthop. J. Sports Med. 8 (12) (2020) 2325967120964919.
[6] B. Tla, B. Tza, B. Wja, et al., Biomimetic strategies for tendon/ligament-to-bone interface regeneration, Bioact. Mater. 6 (8) (2021) 2491–2510.
[7] M. Brown, T. Carter, ACL allograft: advantages and when to use, Sports Med. Arthrosc. Rev. 26 (2) (2018) 75–78.
[8] K. Gao, S. Chen, L. Wang, et al., Anterior cruciate ligament reconstruction with LARS artificial ligament: a multicenter study with 3- to 5-year follow-up, Arthroscopy 26 (4) (2010) 515–523.
[9] Z. Yin, X. Chen, T. Zhu, et al., The effect of decellularized matrices on human tendon stem/progenitor cell differentiation and tendon repair, Acta Biomater. 9 (12) (2013) 9317–9329.
[10] S. Noh, S.J. Lee, J.J. Yoo, et al., Synovium-derived mesenchymal stem cell-based scaffold-free fibrocartilage engineering for bone-tendon interface healing in an anterior cruciate ligament reconstruction model, Tissue Eng. Regen. Med. 21 (2) (2024) 341–351.
[11] A.C. Deymier-Black, J.D. Pasteris, G.M. Genin, et al., Allometry of the tendon enthesis: mechanisms of load transfer between tendon and bone, J. Biomech. Eng. 137 (11) (2015) 111005.
[12] T. Lei, T. Zhang, W. Ju, et al., Biomimetic strategies for tendon/ligament-to-bone interface regeneration, Bioact. Mater. 6 (8) (2021) 2491–2510.
[13] L. Smith, Y. Xia, L.M. Galatz, et al., Tissue-engineering strategies for the tendon/ligament-to-bone insertion, Connect. Tissue Res. 53 (2) (2012) 95–105.
[14] L.Y. Woo, S.D. Abramowitch, R. Kilger, et al., Biomechanics of knee ligaments: injury, healing, and repair, J. Biomech. 39 (1) (2006) 1–20.
[15] M.A. Sinkler, R.J. Furdock, C.J. McMellen, et al., Biologics, stem cells, growth factors, platelet-rich plasma, hemarthrosis, and scaffolds may enhance anterior cruciate ligament surgical treatment, Arthroscopy 39 (2) (2023) 166–175.
[16] Y. Lin, L. Zhang, N.Q. Liu, et al., In vitro behavior of tendon stem/progenitor cells on bioactive electrospun nanofiber membranes for tendon-bone tissue engineering applications, Int. J. Nanomed. 14 (2019) 5831–5848.
[17] B. Yta, C. Cca, D. Fla, et al., Structure and ingredient-based biomimetic scaffolds combining with autologous bone marrow-derived mesenchymal stem cell sheets for bone-tendon healing, Biomaterials 241 (2020) 119837.
[18] S. Chae, Y. Sun, Y.J. Choi, et al., 3D cell-printing of tendon-bone interface using tissue-derived extracellular matrix bioinks for chronic rotator cuff repair, Biofabrication 13 (3) (2021) 33285539.
[19] B.B. Rothrauff, G. Yang, R.S. Tuan, Tissue-specific bioactivity of soluble tendon-derived and cartilage-derived extracellular matrices on adult mesenchymal stem cells, Stem Cell Res. Ther. 8 (1) (2017) 133.
[20] W. Song Zhang, K. Han, et al., Three-dimensional bioprinting of a structure-, composition-, and mechanics-graded biomimetic scaffold coated with specific decellularized extracellular matrix to improve the tendon-to-bone healing, ACS Appl. Mater. Interfaces 15 (24) (2023) 28964.
[21] R. Yang, G. Li, C. Zhuang, et al., Gradient bimetallic ion-based hydrogels for tissue microstructure reconstruction of tendon-to-bone insertion, Sci. Adv. 7 (26) (2021) 3816.
[22] L. Du, J. Wu, Y. Han, et al., Immunomodulatory multicellular scaffolds for tendon-to-bone regeneration, Sci. Adv. 10 (10) (2024) 6610.
[23] C. Yang, G. Deng, W. Chen, et al., A novel electrospun-aligned nanoyarn-reinforced nanofibrous scaffold for tendon tissue engineering, Colloids Surf. B Biointerfaces 122 (2014) 270–276.
[24] S. Bahrami, H. Mirzadeh, A. Solouk, et al., Bioinspired scaffolds based on aligned polyurethane nanofibers mimic tendon and ligament fascicles, Biotechnol. J. 18 (12) (2023) 2300117.
[25] S. Wu, Y. Wang, P.N. Streubel, et al., Living nanofiber yarn-based woven biotextiles for tendon tissue engineering using cell tri-culture and mechanical stimulation, Acta Biomater. 62 (2017) 102–115.
[26] S. Wu, R. Zhou, F. Zhou, et al., Electrospun thymosin Beta-4 loaded PLGA/PLA nanofiber/microfiber hybrid yarns for tendon tissue engineering application, Mater. Sci. Eng., C 106 (2020) 110268.
[27] Y. Xu, J. Wu, H. Wang, et al., Fabrication of electrospun poly(L-lactide-co-ε-caprolactone)/collagen nanoyarn network as a novel, three-dimensional, macroporous, aligned scaffold for tendon tissue engineering, Tissue Eng. C Methods 19 (12) (2013) 925–936.
[28] S. Gupta, S. Majumdar, S. Krishnamurthy, A multifunctional delivery system, J. Contr. Release 335 (2021) 481–497.
[29] A.A. El-Rashidy, J.A. Roether, L. Harhaus, et al., Regenerating bone with bioactive glass scaffolds: a review of in vivo studies in bone defect models, Acta Biomater. 62 (2017) 1–28.
[30] S. Bahrami, A. Solouk, D. Duprez, et al., Microstructure manipulation of polyurethane-based macromolecular scaffold for tendon/ligament tissue engineering, Macromol. Mater. Eng. 307 (1) (2022) 2100584.
[31] C. Yu, T. Wang, H. Diao, et al., Photothermal-triggered structural change of nanofiber scaffold integrating with graded mineralization to promote tendon–bone healing, Adv. Fiber Mater. 4 (2022) 908.
[32] M. Hu, Z. Ling, X. Ren, Extracellular matrix dynamics: tracking in biological systems and their implications, J. Biol. Eng. 16 (1) (2022) 13.
[33] S. Anjum, T. Li, M. Saeed, et al., Exploring polysaccharide and protein-enriched decellularized matrix scaffolds for tendon and ligament repair: a review, Int. J. Biol. Macromol. 254 (2024) 127891.
[34] C. Rinoldi, E. Kijeńska-Gawrońska, A. Khademhosseini, et al., Fibrous systems as potential solutions for tendon and ligament repair, healing, and regeneration, Adv. Healthcare Mater. 10 (7) (2021) 2001305.
[35] C. Jiang, K. Wang, Y. Liu, et al., Application of textile technology in tissue engineering: a review, Acta Biomater. 128 (2021) 60–76.
[36] B.S. Heidari, R. Ruan, E.M. De-Juan-Pardo, et al., Biofabrication and signaling strategies for tendon/ligament interfacial tissue engineering, ACS Biomater. Sci. Eng. 7 (2) (2021) 383–399.
[37] C.P. Laurent, D. Durville, D. Mainard, et al., A multilayer braided scaffold for Anterior Cruciate Ligament: mechanical modeling at the fiber scale, J. Mech. Behav. Biomed. Mater. 12 (2012) 184–196.

[38] M.R. Titchenal, C.R. Chu, J.C. Erhart-Hledik, et al., Early changes in knee center of rotation during walking after anterior cruciate ligament reconstruction correlate with later changes in patient-reported outcomes, Am. J. Sports Med. 45 (4) (2017) 915–921.
[39] A. Kyrkou, S. Dimitris, M. Syrrou, et al., Generation of human induced pluripotent stem cells in defined, feeder-free conditions, Stem Cell Res. 17 (2) (2016) 458–460.
[40] L. Song, R.E. Olsen, J.P. Spalazzi, et al., Biomechanical evaluation of acellular collagen matrix augmented Achilles tendon repair in sheep, J. Foot Ankle Surg. 49 (5) (2010) 438–441.
[41] Z. Pan, H. Yin, S. Wang, et al., Potential in vitro tissue-engineered anterior cruciate ligament by copolymerization of polyvinyl alcohol and collagen, J. Craniofac. Surg. 32 (2) (2021) 799–803.
[42] J. Zheng, F. Zhao, W. Zhang, et al., Sequentially-crosslinked biomimetic bioactive glass/gelatin methacryloyl composites hydrogels for bone regeneration, Mater. Sci. Eng., C 89 (2018) 119–127.
[43] J.L. Koh, Z. Szomor, G. Murrell, et al., Supplementation of rotator cuff repair with a bioresorbable scaffold, Am. J. Sports Med. 30 (3) (2002) 410–413.
[44] S.F. Hanum Aminatun, R.D. Izak, et al., Fabrication and compatibility evaluation of polycaprolactone/hydroxyapatite/collagen-based fiber scaffold for anterior cruciate ligament injury, RSC Adv. 13 (16) (2023) 10459–10467.
[45] Y. Liu, Q. Guo, X. Zhang, et al., Progress in electrospun fibers for manipulating cell behaviors, Adv. Fiber Mater. 5 (2023) 1241–1272.
[46] X. Zhang, M. Guo, Q. Guo, et al., Modulating axonal growth and neural stem cell migration with the use of uniaxially aligned nanofiber yarns welded with NGF-loaded microparticles, Mater. Today Adv. 17 (2023) 100343.
[47] Y. Tang, J. Tian, L. Li, et al., Biomimetic biphasic electrospun scaffold for anterior cruciate ligament tissue engineering, Tissue Eng. Regen. Med. 18 (5) (2021) 819–830.
[48] C. Emonts, D. Wienen, B. Bauer, et al., 3D-Braided poly-ε-caprolactone-based scaffolds for ligament tissue engineering, J. Funct. Biomater. 13 (4) (2022) 230.
[49] F. Bi, Y. Chen, J. Liu, et al., Anterior cruciate ligament reconstruction in a rabbit model using a silk-collagen scaffold modified by hydroxyapatite at both ends: a histological and biomechanical study, J. Orthop. Surg. Res. 16 (1) (2021) 139.
[50] P. Zhang, F. Han, T. Chen, et al., "Swiss roll"-like bioactive hybrid scaffolds for promoting bone tissue ingrowth and tendon-bone healing after anterior cruciate ligament reconstruction, Biomater. Sci. 8 (3) (2020) 871–883.
[51] T. Wu, H. Li, J. Xue, et al., Photothermal welding, melting, and patterned expansion of nonwoven mats of polymer nanofibers for biomedical and printing applications, Angew. Chem. In. Edit. 58 (2019) 16416–16421.
[52] Z. Feng, X. Zhang, N. Liu, et al., Promotion of neurite outgrowth and extension using of injectable welded nanofibers, Chem. Res. Chin. Univ. 37 (2021) 522–527.
[53] M.P. Prabhakaran, J. Venugopal, S. Ramakrishna, Electrospun nanostructured scaffolds for bone tissue engineering, Acta Biomater. 5 (8) (2009) 2884–2893.
[54] E. Maurice, A.L.R. Rangel, J.K. Venkatesan, The effect of pNaSS grafting of knitted poly (??-caprolactone) artificial ligaments on in vitro mineralization and in vivo osseointegration, Materialia 21 (2022) 1, 101331.
[55] S. Taketomi, Editorial commentary: tunnel widening after anterior cruciate ligament reconstruction may increase laxity and complicate revision, Arthroscopy 37 (2021) 2564–2566.
[56] X. Guo, M. Li, W. Qi, et al., Serial cellular events in bone formation initiated by calcium phosphate ceramics, Acta Biomater. 134 (2021) 730–743.
[57] S.A. Shah, I. Kormpakis, N. Havlioglu, et al., Sclerostin antibody treatment enhances rotator cuff tendon-to-bone healing in an animal model, J Bone Joint Surg. Am 99 (10) (2017) 855–864.
[58] Z. Yang, Z. Yang, L. Ding, et al., Self-adhesive hydrogel biomimetic periosteum to promote critical-size bone defect repair via synergistic osteogenesis and angiogenesis, ACS Appl. Mater. Interfaces 14 (32) (2022) 36395–36410.
[59] D. Qu, C.Z. Mosher, M.K. Boushell, et al., Engineering complex orthopaedic tissues via strategic biomimicry, Ann. Biomed. Eng. 43 (2015) 697–717.
[60] A.H. Huang, H.H. Lu, R. Schweitzer, Molecular regulation of tendon cell fate during development, J. Orthop. Res. 33 (2015) 800–812.